Mechanical Properties and Corrosion Resistance of Mechanically Alloyed Fe-based Nanostructures Consolidated by Spark Plasma Sintering

A DISSERTATION

Submitted in partial fulfillment of the

Requirements for the award of the degree

Of

MASTER OF TECHNOLOGY

In

METALLURGICAL AND MATERIALS ENGINEERING

(With Specialization in Materials Engineering)

By

ARPAN ARORA

(Enrolment No: 15545004)

DEPARTMENT OF METALLURGICAL AND MATERIALS ENGINEERING

INDIAN INSTITUTE OF TECHNOLOGY ROORKEE

ROORKEE – 247667 (INDIA)

Nov-2017

CANDIDATE'S DECLARATION

I hereby declare that the proposed work presented in this dissertation entitled '**Mechanical Properties and Corrosion Resistance of Mechanical alloyed Fe-based Nanostructures Consolidated by Spark Plasma Sintering'** in partial fulfillment of the requirements for the award of the degree of **Master of Technology** in '**Metallurgical and Materials Engineering'** with specialization in **Materials Engineering**, submitted in the **Department of Metallurgical and Materials Engineering**, '**Indian Institute of Technology Roorkee'** is an authentic record of my own work carried out during the period from July 2015 to June 2016, under the supervision of Dr. Suhrit Mula, Assistant professor, and Dr. B.V. Manoj Kumar, Associate Professor, Department of Metallurgical and Material Engineering, Indian Institute of Technology Roorkee.

The matter presented in this dissertation has not been submitted anywhere in any form by me for awarding any degree.

Dated:

Place: Roorkee **(ARPAN ARORA)**

CERTIFICATE

This is to certify that the above statement made by the candidate is correct to the best of my knowledge and belief.

Dr. Suhrit Mula Dr. B.V. Manoj Kumar

(Supervisor) (Supervisor)

ACKNOWLEDGEMENTS

I owe my sincere gratitude to my guides **Dr. Suhrit Mula,** Assistant professor, Indian Institute of Technology, Roorkee and **Dr. B.V. Manoj Kumar**, Associate Professor, Metallurgical and Materials Engineering, IIT, Roorkee. Without their untiring mentorship, constant inspiration, valuable discussions and suggestions, this report would not have been possible. They patiently provided the vision, encouragement and advice necessary for me to proceed through the entire research program.

I take the opportunity to specially thank Mr. V.M. Suntharavel Muthaiah PhD scholar, MMED and M.Tech. student Mosses JP, for helping me throughout my work and tackling all the challenges during my experimental work.

I would also like thank Metallurgical and Materials Engineering for allowing me to use the equipment's for performing all the experiments.

(ARPAN ARORA)

CONTENTS

LIST OF FIGURES

List of Tables

ABSTRACT

In the present work, iron, nickel and nano sized (20-30 nm) powders with compositions 42wt.%Ni, Fe-42wt.%Ni-2wt.%Y_2O_3 and Fe-2wt.%Y_2O_3 were prepared by high energy ball milling. The miilled samples were sintered by spark plasma sintering (SPS) at 800, 900 and 1000°C in argon atmosphere with a holding period of 5 min at a pressure of 60 MPa. The density of the sintered alloys increased from 78% at 800^{o}C to 98% at 1000^{o}C. XRD analysis indicates the presence of Fe-Ni phase in sintered the Fe-Ni alloy, while additional presence of intermetallic phases (Ni_5Y, $Fe_{17}Y_2$) and oxides (NiO, Fe_3O_4) observed in the sintered Fe-Y_2O_3 and Fe-Ni-Y_2O_3 alloys. The microstructures of the alloys sintered at 1000^{o}C revealed decrease in average grain size from ~10 µm for Fe-Ni to ~1 µm for Fe-Y_2O_3 and ~500 nm for Fe-Ni-Y_2O_3. The nanoindentation hardness of the sintered alloys varied from 5.8 GPa for Fe-Ni to 7.2 GPa for Fe-Y_2O_3 and 7.9 GPa Fe-Ni-Y_2O_3. Sliding wear tests in dry conditions against alumina ball indicate that average coefficient of friction varied from 0.5 (Fe-Ni-Y_2O_3) to 1.7 (Fe-Ni) and depth of wear track varied from 5 µm to 20 µm with change in composition of the alloy and sliding load (from 5 to 20 N). The presence of oxide rich layer at the contact surface is found responsible for less coefficient of friction and depth of wear track for the Fe-Ni-Y_2O_3 alloy. Corrosion tests in 3%NaCl indicate decreased corrosion density (I_{corr}) from 1.34 µA/cm^2 for Fe-Ni and 0.78 µA/cm^2 Fe-Ni-Y_2O_3. The present research work essentially indicates a significant grain refinement with subsequent improvement of mechanical, wear and corrosion properties due to the addition of nano sized ytrria in iron-nickel alloy.

Keywords: Ball milling, Spark plasma sintering, Mechanical properties, Wear, & Corrosion,

CHAPTER 1 INTRODUCTION

Iron is the commonly found element on earth. Owing to the unique combination of properties like high strength, superior magnetic properties, iron is preferred for wide variety of applications including structural, magnetic and automobile applications. The mechanical and corrosion properties can be improved by alloying with suitable elements. Fe-Ni alloys have excellent mechanical, wear, thermal and magnetic properties and can be produced in large quantities. It can also be produced in a variety of forms and forms, including thin coatings, self-supporting sheets, tubes and foils, and complex geometries. Among all the known alloying elements, Ni has gained attention of many researchers due to its versatile behaviour. It improves the chemical inertness, mechanical behaviour, phase formation and toughness of iron based materials [26]. For example, Fe-2wt.%Ni has been reported to exhibit high wear resistance and better mechanical behavior [26]. Invar (containing 36%Ni) and super invar (containing 42%Ni) are known for their mechanical strength and low coefficient of expansion [26]. Fe-50Ni (containing 50% Ni) has superior magnetic behaviour [26]. The Ni added alloys also show a good room temperature corrosion resistance in certain electrolytes [26]. As Ni is γ-stabilizer in iron, it alters the fcc to bcc transition temperature and helps in commercial austenitic steel, but the addition of Ni to Fe has little effect on stabilizing grain growth [15]. On the other hand, increasing the fraction of Ni in Fe-Ni alloy causes decrease in corrosion rate as well increase in wear rate [26].

Fe−Ni-oxides nanocomposites have a large number of applications such as catalysts, recording heads, shielding of magnetic materials, high performance transformers as well as, used in high temperature structural materials due of their excellent corrosion and oxidation resistance, high strength and fracture toughness, good magnetic properties, and good wear resistance.[19]. The addition of ultrafine oxide particles (usually Y_2O_3) retards the recrystallization, grain coarsening, and grain boundary sliding thereby significantly improves the creep strength [18]. There is reduction in oxidation rate and enhance adhesion between oxide scale and substrate, due to which exfoliation resistance of oxide scale increase[25] It was also find that the addition of Y_2O_3 can increase the toughness of structurally amorphous metal. [27] In addition, the Y_2O_3 acts as better stabilizer that can restrict the grain growth through the phase transformation at high temperature ($T \geq 900°C$) [16].

Many techniques are used to produce nanostructured materials such as (a) inert gas condensation, (b) rapid coagulation processes, (c) position electrode (d) sputtering, (e) crystallization of amorphous phases (f) a chemical reaction and (g) mechanical wear (ball milling / mechanical alloy) [7]. Mechanical alloying has the ability to synthesize a variety of metastable phases ranging from elemental powder mixtures to pregelatinized powders with ductile-ductile or brittle-brittle combinations of materials. Unlike many of the above methods, mechanical wear does not produce nanostructures by cluster assembly, but due to structural decomposition of coarser structures as the result of severe plastic deformation [7].

The consolidation of powder mixtures by spark plasma sintering allows achieving high densities with considerable restriction in grain coarsening. However, preparation of iron-nickel-yttria alloys by spark plasma sintering and the characterization of sintered alloys are not considerably explored. In this context, iron, nickel and nano sized (20-30 nm) powders with compositions 42wt.%Ni, Fe-42wt.%Ni-2wt.%Y_2O_3 and Fe-2wt.%Y_2O_3 as shown in **Table 1.1** were mixed by high energy ball milling and consolidated by spark plasma sintering (SPS) at 800°, 900° and 1000°C for 5 min at 60 MPa in argon atmosphere. The microstructural, wear and corrosion characteristics were studied.

Table 1.1 Compositions of prepared alloys.

Designation	**Fe**	**Ni**	**Y_2O_3**
Fe-Ni	58	42	-
Fe-Y_2O_3	98	-	2
Fe-Ni-Y_2O_3	56	42	2

1.1 Objectives

The following are the major objectives of the present study:

(i) To prepare dense Fe-Ni, Fe- Y_2O_3 and Fe-Ni- Y_2O_3 alloys in optimum conditions of spark plasma sintering

(ii) To study microstructural features and phase evolution of the sintered alloys

(iii) To understand the effect of nano size yttria on the hardness and wear behaviour of sintered alloys

(iv) To estimate the corrosion performance of the sintered alloys

1.2 Structure of the thesis

To envisage the above mentioned objectives, the thesis is structured as per the following:

Chapter-2 Literature review

A review of the published available literature in areas that are directly relevant to the present study is presented in this chapter.

Chapter-3 Experimental details

Details including powders used, compositions investigated, spark plasma sintering are explained. This is followed by details of density measurement, phase analysis, microstructural characterization, hardness, wear and corrosion property measurement of the investigated alloys.

Chapter-4 Results and Discussion

In this chapter, a discussion on major results obtained in preparation and characterization of investigated alloys is provided. First, results obtained from mechanical alloying and spark plasma sintering are discussed. This is followed by detailed discussion on microstructural characteristics, wear and corrosion behavior of sintered iron-based alloys

Chapter-5 Conclusions and future scope

Important conclusions drawn from the present thesis work and future directions are suggested in this chapter.

CHAPTER 2 LITERATURE REVIEW

Iron is well known and useful metal due to its low cost, high strength and availability. It various applications are automotive, structural applications, magnet of manufacturing and many other home applications. So, it requires improving the properties of iron or iron based alloys. Properties can be enhanced by manufacturing of nanostructured iron and a solid solution of iron with other materials such as, chromium, nickel etc. The ultrafine oxide particles of Y_2O_3 delayed the recrystallization, grain coarsening and grain boundary sliding therefore significantly improves the creep strength [18]. It was also concluded that addition of Y_2O_3 can enhance the toughness of structurally amorphous metal (SAM) [27]. It is expected that Y_2O_3 is better stabilizer that can restrict the grain growth through the phase transformation as well as at high temperature ($T \geq 900°C$) [16].

High energy ball milling helps the production of nanostructured material, resulting in powdery samples with different structures and new properties. Due to their small grain size, these materials are characterized by the relatively high number of atoms in the grain boundary. In addition, they are very interesting from a magnetic point of view, because the size of the grains is close to a magnetic domain and there is therefore the possibility of eliminating the influence of the walls of the domain. It is well known that intermetallic mechanical alloy compounds are highly disordered and not stable [6]

2.1 Different techniques for synthesis of nanostructured materials

Nanostructure material can be produce by several techniques. (a) Inert gas condensation, (b) Rapid coagulation processes, (c) Position electrode (d) Sputtering, (e) Crystallization

of amorphous phases (f)A chemical reaction and (g) Mechanical milling/alloying [7]. In Mechanical alloying (MA) nanopowder is homogeneously mix at atomic level, breaking and re-welding of powder particles in a high energy ball mill. The synthesized non-equilibrium phases include supersaturated solid solution, metastable crystalline and semi-crystalline phases, nanostructures and amorphous alloys. Recent developments in these areas as well as the clutter ordered intermetallic compounds and mechano-synthesis of materials critically after discussing process and process variables that play a role MA [8].

2.2 Mechanism of alloying

During grinding, when two hard balls are in danger, they have a small amount of powder in the charge. Normally, about 1000 particles are picked up during each collision (Figure 2.1). Influence force substantially deforms the powder particles as it works hard and breaks. With the new generated surfaces, the particles can be seen together and, as a result, an increase in particle size occurs in the case of a ductile or ductile-brittle material mixture. At this point, the composite particles (Figure 2.2) characterize characteristic structures consisting of different combinations of starting components.

With continuous deformation, the particles harden fragile or fragmented by fragile flakes. At this point, the tendency to break over the most cold welding is high. Due to the continued impact of the grinding balls, the particle structure is filtered consistently, but the size of particles is the same after a certain grinding time. A stationary balance is achieved when a balance between the cold welding rate and the rate of breaking is achieved. At this stage, all of the initial components in each particle are in the same ratio of the original composition. During the MA, some crystallises are introduced, such as

disabilities, vacancies, stroke defects, and increased number of grain limits. During the MA with a variety of solute elements in the matrix, it enhances the faults such as mitigations, vacancies, steel defects etc. The interconnection distance is also reduced due to the mitigation of micro-infrastructure. In addition, the slight increase in the temperature of the material also helps milling in circulation. As a result, the alloy formation is true among the ingredients [9].

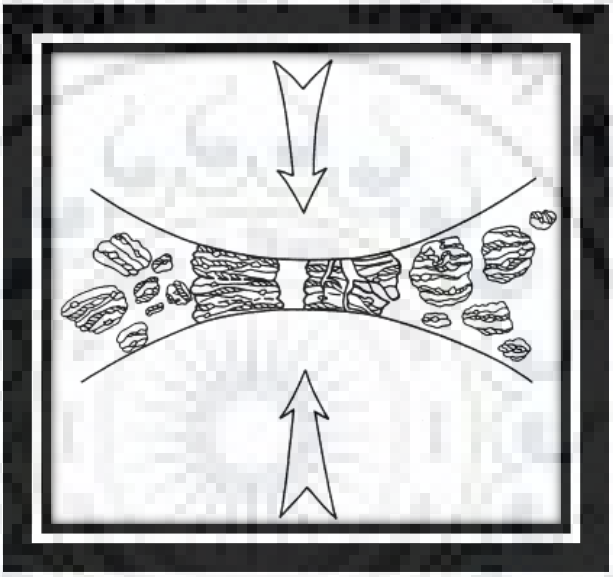

Fig. 2.2(a). Ball-powder-Ball collision of powder mixture during MA (Ref. [10]).

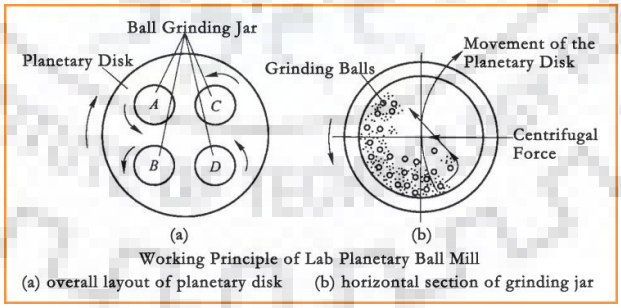

Fig. 2.2(b): Ball-powder-Ball mechanism in planetary ball milling (Ref. [10]).

In a ball mill, the centrifugal force produced by the vial is rotated around their axes and produces both the rotary support disk acting on the material of the vial, which consists of material such as milling and grinding balls. Since the vials and the support disc are in other directions, the centrifugal forces will alternately act on similar instructions. This means that the balls grind inside the bottle wall - the friction effect and subsequent material and dispose of grinding balls and travel freely through the inner chamber of the vial and against the inside of the inner wall - impact effect (Fig. 2.2).

2.3 Process variable

There are several parameters as required to be chosen carefully before milling

- Container of milling
- Speed of milling in rpm
- Time for milling in minutes
- Ratio for Ball to powder
- Filling of vial
- Atmosphere for milling
- Process control agent
- Temperature of milling

Up to some extent all processes are dependent to each other. For example, the size of the grinding medium, optimum milling depends on the type of mill, the ratio of ball to powder, temperature of the grinding etc. [6]

2.3.1 Type of mill

Type of mill depends on the requirement, like product, quantity of product, availability of facilities, factories. SPEX shaker as shown in **fig.2.3(a)** is most commonly used for alloy

testing. For large quantity of powder generally The Attritor mills and Fritsch Pulverisette planetary ball as **shown in fig 2.3(b)** mills are used. For special application special mills are design[6]

(a) High energy ballmilling (b) Planetary ballmilling

Fig. 2.3: High energy ball milling and planetary ball milling

2.3.2 Milling container

Milling container is selected on the several parameters like, hardness of material, grip, contaminations factor, machine, chemical reaction. The hardness of milling material should be less than the container otherwise contamination of container will also joint with material. Inside surface should be smooth to minimised the contamination. There should not be chemical reaction between the material and container. In planetary ball mill the container weight should be balanced else the vibration may affect the milling. Most commonly used contains are: stainless steel, WC-Co, Hardened steel, tool steel, hard chrome steel.[6]

2.3.3 Ball-to-powder weight ratio (BPR)

The ratio of bale weight to powder (BPR), sometimes called the tax ratio (CR), is an important variable in the milling process. The minimum BPR varies between 1: 1 and 220: 1. Generally, the ratio of 10: 1 is most used when the powder is sent to a small capacity mill such as an SPEX mill. But when the mill is greater than 50: 1 or even 100: 1 is used. The ratio of the weight of the powder to the 10: 1 powder was used for the present study.

2.3.4 Filling the vial

As the alloy is produced between the dust/powder particles as a result of the impact forces applied there to, it is necessary that there is enough space for the balls and dust/powder particles to move freely there. The grinder Therefore it is important to fill the bottle with the powder and the pearls. Therefore, it should be noted that the vial does not get too fill, usually about 50% of the contents of the vial are left blank.

2.3.5 Atmosphere for milling

Various atmospheres were used during milling for specific purposes. Nitrogen or ammonia atmospheres were used to make nitrides. A hydrogen atmosphere was used to generate hydrides. It has been shown that the presence of air in the ampule produces oxides and nitrides in the powder, especially when the powders are reactive. Therefore, it is important to use an inert atmosphere during milling.

2.4 Addition of Y_2O_3

Zr intermetallic bases and ex-substituted Y_2O_3 secondary phases, both are essential for a combination of high thermal stability and high mechanical hardness. At higher temperatures, the deposited secondary phase particles become coarse, reducing the

stabilizing effect along with the strength of the material [16]. The reduction of crystal size acceleration and the formation of solid solutions was observed in the ODS alloy due to the presence of nanotyplatide particles. During MA, a solid solution of bcc was first observed and converted into a solid FCC solution with continuous milling. After changing the grain size from 5 nm to 110 nm, the apparent hardness is given as 530 and 900 HV [18].

2.5. Effect of sintering temperature

The sintering process at a temperature of 600°C gave a solid solidified sample of SAM 7-2.5 wt% Y_2O_3. X-ray diffraction shows that neither the addition of Y_2O_3 nanoparticles during milling nor the sintering process themselves lead to devitrification of the materials. [11]. Discover the influence of different MA time and SPS temperature on Y_2O_3 stability and sintering behavior. It is analyse that the MA time does not affect the sintering behavior of Fe ODS-based alloys. The best prerequisite for the production of ODS alloys based on pure Iron was SPS at 1100°C and the MA time 90 minute [12].

Grain growth stabilized in Fe-Ni alloys. Microstructural evolution is slow and stable stabilization to 700°C. Over 700°C, grain growth is very fast, especially during the first few seconds of annealing. The cause of abnormal growth and loss of thermal stability has been identified as the appearance of the fcc-Y phase and the subsequent reduction in the total area of the grain boundaries and the total stored energy in the sample [14].

Up to 600°C, the Fe91Ni8Zr1 microstructure or alloy at the nanoscale less than 15 nm, released at 700°C, increases grain growth or ternary alloy abnormally but remains below 100 nm. At higher glow temperature, zener pinning of Fe_2Zr_1 grain boundaries at high

temperatures. The results of the microhardness and punching test show that the particle strengthening contributes greatly to the gain of $Fe91Ni_8Zr1$ at high temperature [15].

Intensity of peak was observed same for both temperatures [17]. As sinter temperature increases, density increases. At 950°C, the type of fracture was intergranularly pure, while at 1230°C, transgranular fracture was catering. No effect was shown in XRD analysis. The intensity of peak was the same for both of them [17].

CHAPTER 3 EXPERIMENTAL DETAILS

This chapter describes details of the experimental procedures performed in this study. Mechanical milling to reduce as received ytrria and to mix with appropriate amounts of iron, nickel and yttria is described. The spark plasma sintering is explained. The phase analysis, microstructural characterization, hardness, wear and corrosion property measurement of the investigated alloys are described.

3.1 Mechanical milling

As received Y_2O_3 powder (99.0% purity with initial size of 44µm, purchased from Alfa-Asear) was milled to reduce size by planetary ball milling (Retsch, PM400, Germany) using a tungsten carbide pot and tungsten carbide balls with a ball to powder ratio of 10: 1. The grinding was done for 40 hours at 270 rpm. Milling was conducted in toluene to control the generated heat. A photograph of planetary ball mill used for the study is shown as **Fig.3.1.**

Fig.3.1(a): Planetary ball mill Retsch PM 400

As received iron (size 325 mesh, with 98% purity purchased from Alfa Aesar) was milled in high energy ball mill (Spex 8000M, USA) for 24 h in carbide steel vial and carbide steel balls with a ball to powder weight ratio of 10:1. Milled yttria, milled iron and nickel (size 100 mesh, 95% purity, purchased from Himedia) were used to prepare three compositions: Fe-42 wt% Ni, Fe-2 wt% Y_2O_3, and Fe-42 wt% Ni-2 wt% Y_2O_3. These compositions are respectively designated as Fe-Ni-Y_2O_3, Fe-Ni and Fe-Y_2O_3. The carbide steel vials containing powder mixtures were filled with argon in a glove box for 15 min. The powder mixtures were milled by high energy ball milling (Spex 8000M, USA) in carbide steel vial and carbide steel balls with a ball to powder weight ratio of 10:1. Mixing was done at 1725 rpm for 1500 min. A photograph of the high energy ball mill is shown as **Fig. 3.1(b).**

Fig. 3.1(b): Spex 8000M Ball Mill, (Carbide Steel mill sets)

3.2 Spark Plasma Sintering

All the powder mixtures were kept in a graphite punch of 10 mm diameter and sintered in a spark plasma sinter (SPS 625, Dr. Sinter, Fuji Electronics Ltd., Japan) in argon atmosphere at 60 MPa pressure and three different temperatures: 800^{o}C, 900^{o}C, 1000^{o}C for 5 min. Rate of heating was maintained at 100^{o}C/min. A photograph of spark plasma

sintering (SPS) furnace is shown as **Fig. 3.2**. The sintered specimens had dimensions of 10 mm diameter and 2 mm thickness. The density of sintered specimens was measured by Archimedes method using distilled water.

Fig. 3.2.Spark plasma sintering (SPS) machine

3.3 Phase analysis

The powders and powder mixtures were subjected to X-ray diffraction using a D8-Advance Bruker, Diffractometer fitted with goniometer with Cu-Kα radiation of wavelength 0.154 nm and polished samples of sintered specimens subjected to X-ray diffraction using a Philips X-pert MPD X-ray diffractometer (**Figure 3.3)** fitted with goniometer with Co-Kα radiation of wavelength 0.179nm at 0.5^{o}/min. to identify

different phases. An Expert High Score Plus^{TM} software with inbuilt JCPDS (Joint Committee on Powder Diffraction Standards) was used to index peaks of various phases.

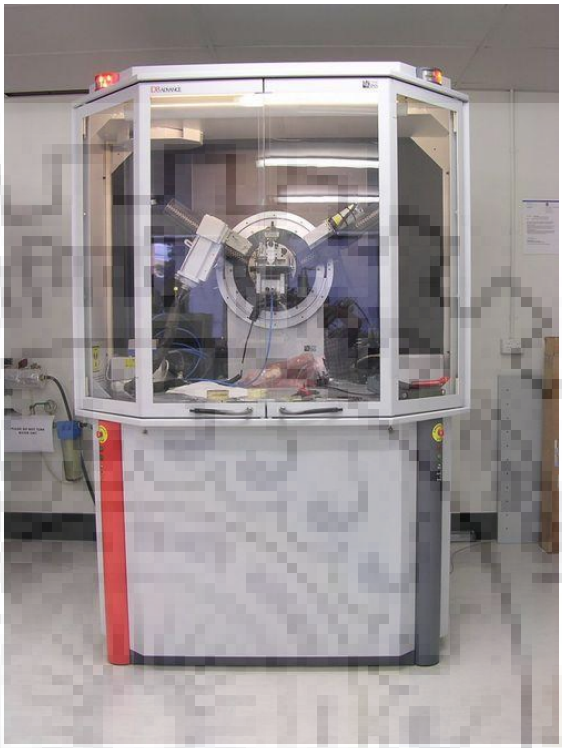

Fig. 3.3. X-Ray Diffraction machine

3.4 Microstructural characterization

The surfaces of the sintered alloys were prepared using standard techniques involving cloth polishing with successively finer grades of emery papers. Polished surfaces were subjected to etching using Nital (5% HNO_3 and 95% Ethanol) for 3-15 s. Microstructures of etched surfaces were observed using a optical microscope (Leica, 500M, Germany).

A scanning electron microscope (FESEM, Quanta 200 FEG, the Netherlands) equipped with an energy dispersive X-ray spectroscope (EDS, Oxford Instruments, UK) was used to study microstructural features of powder mixtures and sintered specimens. A photograph of scanning electron microscope is shown in **Fig. 3.4.**

Fig. 3.4. Scanning Electron Microscope

3.5 Hardness Measurement

Bothe micro hardness and nano hardness of the sintered specimens were measured. A Vickers hardness tester (Leco LV 700, USA) was used to determine the Vickers hardness values of all sintered samples using a 50 gram load for a residence time of 5 seconds.

Fig. 3.5(a). Leco LV 700 Vickers hardness tester

The nano hardness measurement was done to study the hardness of iron or iron-nickel grains using a Triboindenter (Hysitron TI950 Hysitron Inc, USA) equipped with three-sided Berkovich diamond indenter with a tip radius of 100 nm. A maximum normal load

of 5000μN was applied at 400 μN/s for 2 s. A photograph of nano hardness tester is shown as **Fig. 3.5(b)**

Fig. 3.5(b): Hysitron TI 950 for Nanoindentation test

3.6 Wear behavior evaluation

The wear behavior of sintered specimens was studied against commercially available alumina balls (Vickers hardness of 16 GPa, as per the vendor RGP Balls) of 10 mm diameter in dry conditions using a ball-on-disk tribometer (TR-201E-M2, DUCOM, Bangalore, India). The alumina ball was kept stationary and sintered alloy sample was rotated at 500 rpm to make track radius of 5 mm for 30 min under different loads: 5, 10 and 20 N in ambient conditions (Room temperature and 45 -50% RH). The frictional force was recorded online and the coefficient of friction was generated. A photograph of wear tester is shown in **Fig 3.6**. A stylus-tip profilometer (T800 Mitutoya, Japan) was used to analyze the surface of worn alloys. Surface profiles were used to measure the depth of wear track in transverse direction to the sliding direction. At least six measurements were taken to represent average depth for each worn alloy. Also, worn surfaces of investigated alloys were examined to identify the dominant wear mechanisms using scanning electron microscopy (SEM)/Energy dispersive spectroscopy (EDS).

Fig. 3.6. Ball on disk wear tester

3.7 Corrosion behavior

Corrosion behavior of Fe-Ni and Fe-Ni-Y_2O_3 alloys was studied in a round bottom cell with saturated calomel electrode as the reference electrode. Tests were conducted in freely aerated 3.5% solution of NaCl electrolyte. A photograph of the cell is provided as Fig.3.7. Tafel extrapolation analysis was used to determine the corrosion rate. Each test was performed twice to check the reproducibility of the electrochemical polarization behavior.

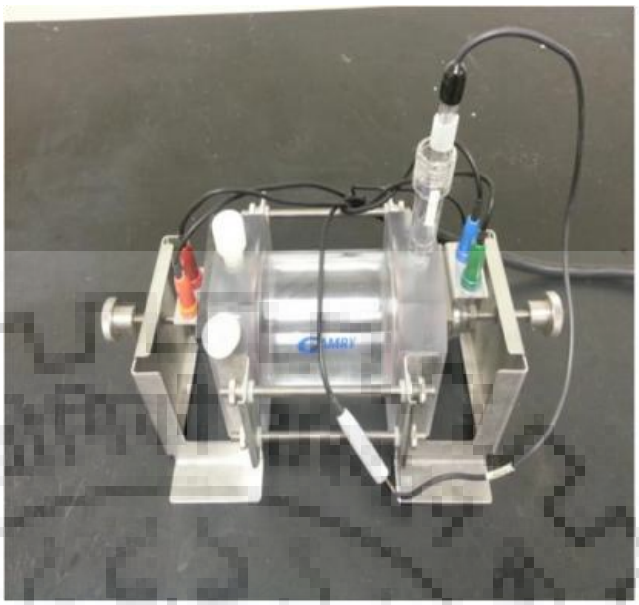

Fig. 3.7: The round bottom cell used for corrosion tests

CHAPTER 4 RESULTS AND DISCUSSION

In this chapter, major results obtained from different experimental sections are discussed. First, the results obtained from characterization of powders, ball milling and spark plasma sintering are discussed. This is followed by discussion on results obtained from characterization of sintered alloys, wear and corrosion studies.

4.1 Size reduction of Y_2O_3 powder and mechanical alloying

As received yttria powder of 40 µm size was milled in a planetary ball mill for 40 h. **Fig. 4.1** shows images of yttria powder after 20h and 40 h milling. The average size of the yttria powder reduced to around 1 um after 20h milling, while it reduced to 20-30 nm after milling for 40h. Further, agglomeration of powders is evident. The agglomerates were broken by ultrasonication. The milled iron, milled yttria and nickel powders were mixed in a high energy ball mill.

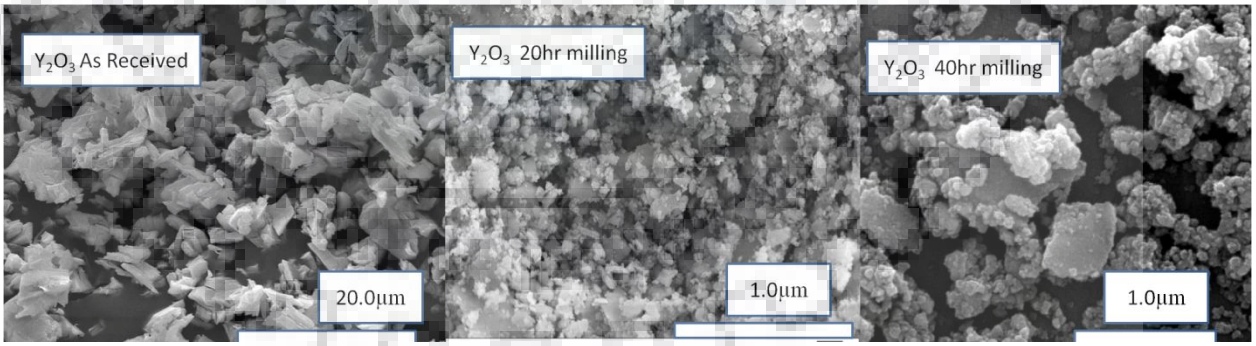

Fig. 4.1 As received, 20 h milled and 40 h milled yttria (Y_2O_3) powder particles.

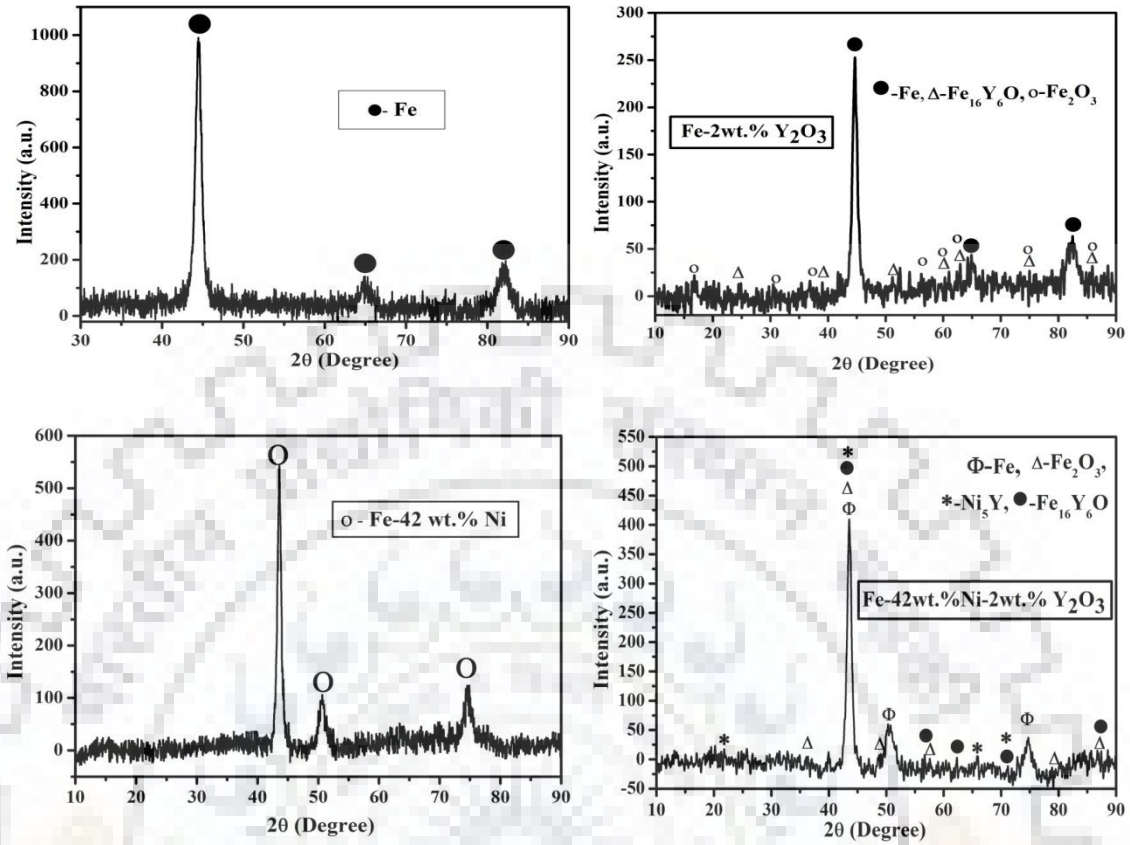

Fig. 4.2 XRD analysis of Fe, Fe-42wt. % Ni & Fe-42wt. %Ni -2wt.%Y_2O_3 and Fe-2wt.%Y_2O_3 milled powder

The phase analysis of mixed powder compositions are shown in **Fig. 4.2**. XRD analysis of milled iron powder (99.9%) shows only one phase of iron peak, but the formation of Fe-Ni is found when 42wt% Ni is added to iron powder. Further, $Fe_{16}Y_6O$, Fe_2O_3 and Fe phases are found with the addition of Y_2O_3 in iron powder. 10]. On the other hand, the XRD analysis of Fe-42 wt% Ni-2wt% Y_2O_3 powder mixture reveals the formation of Ni_5Y in addition to Fe, Fe_2O_3, and $Fe_{16}Y_6O$. Thus, the addition of small amount of Y_2O_3 powder in Fe or Fe-Ni powder mixture leads to the formation of intermetallic and oxides. [10]

4.2. SPARK PLASMA SINTERING

Typical spark plasma sintering (SPS) profiles between Temperature Time and Displacement for the investigated compositions are shown in **Fig. 4.3.** As the temperature is increased, the displacement increased. For a given alloy, larger displacement .is found when sintered at high temperature of1000^{o}C|.

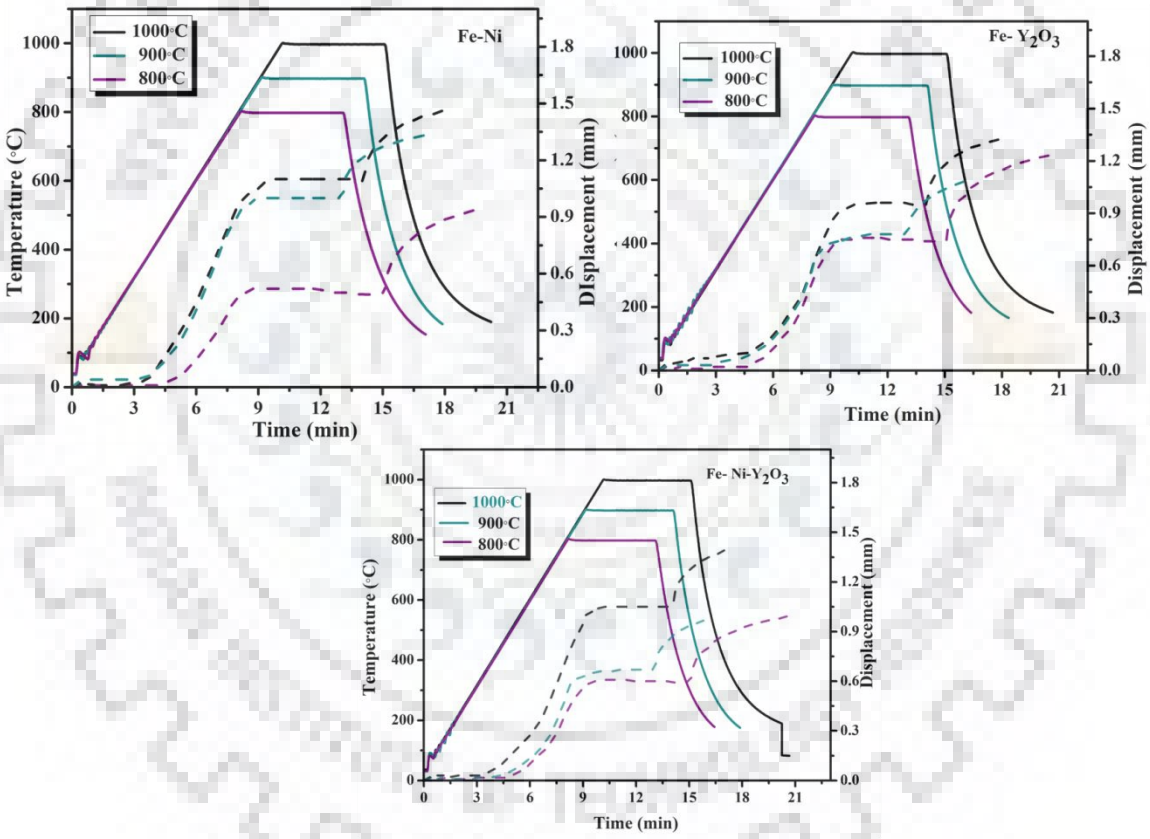

Fig. 4.3 Spark plasma sintering profiles between temperature, time and displacement for the investigated compositions.

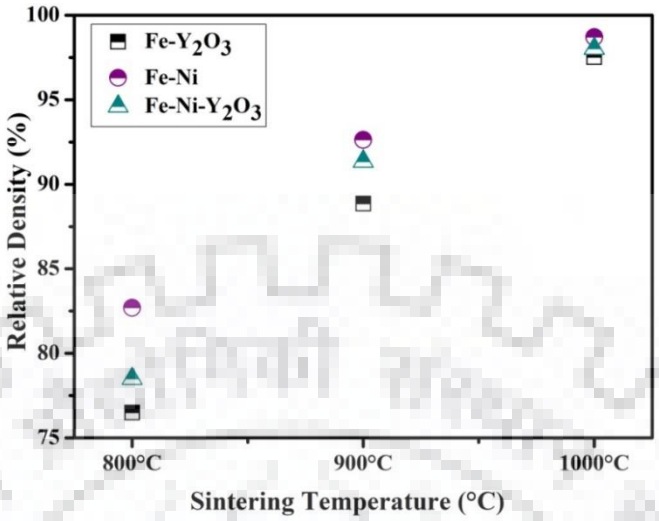

Fig. 4.4 Density graph of SPS sample

Relative density of the investigated alloys sintered at different temperatures is shown in **Fig. 4.4** The density of alloys sintered at 800°C was found least (76%) for Fe-42Ni-2(Y_2O_3) alloy. As the sintering temperature was increased to 1000°C maximum density of 98.5% is observed in case of Fe-42Ni. The average density prepared through the powder metallurgy process increases with increase in sintering temperature. It is mainly due to the decrease in the total fractional porosity of the sample with the increase in the sintering temperature. [17] [21].

4.3. Phase analysis sintered sample

XRD analysis of Fe-Ni, Fe-Y_2O_3 and Fe-Ni-Y_2O_3 alloys sintered at three different temperatures (800°C,9 00°C and 1000°C) show various phases (see **Fig. 4.5**). In Fe-Ni alloy, the peak identified matched only with Fe-Ni alloy, while no other intermetallic or oxide formation is detected. No change is observed with change in sintering temperature. Fe phase is identified in Fe-Y_2O_3 alloy and and Fe-Ni phase in Fe-Ni-Y_2O_3 alloy.

However, intemetallics $Fe_{17}Y_2$ and Ni_5Y are observed in Fe-Ni-Y_2O_3 and Fe-Y2O3 alloys respectively. In addition, oxides Fe_3O_4 is found in both alloys. Further, the NiO is observed in Fe-Ni-Y_2O_3 alloy. Thus, the formation of new oxides and intermetallic is observed in sintered alloy as compared to powder mixtures.

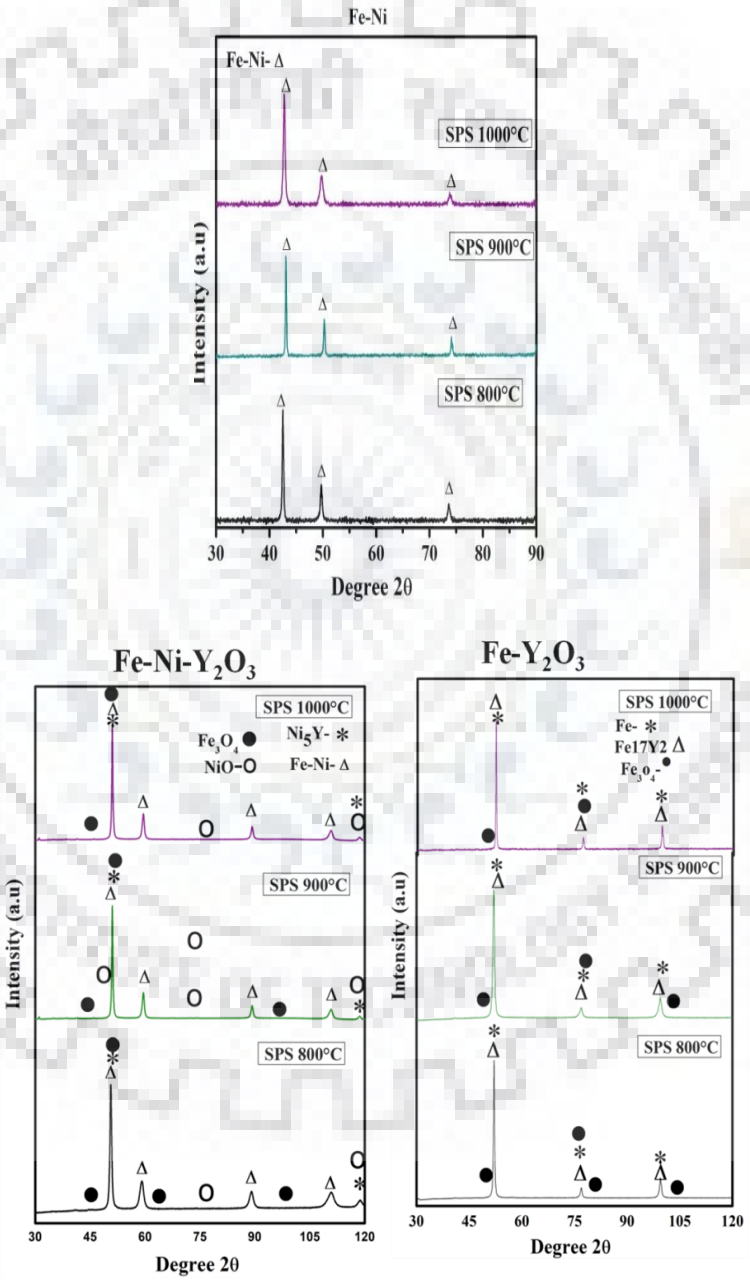

Fig. 4.5 XRD analysis of Fe-42wt. % Ni & Fe-42wt. %Ni -2wt.%Y_2O_3 Sintered sample

4.4. Microstructural characterization

The etched microstructures of investigated alloys sintered at different temperatures are shown in **Figs. 4.6** through **Fig. 4.11**. In general, microstructures of alloys sintered at 800^{o}C showed agglomeration and considerable porosity. The grain size was fairly homogeneous at a given temperature but increased with increase in temperature. At 900 °C, the formation of necks between particles is observed which led to the development of grains. Further, small, irregular and rounded morphology of grains is observed when sintered at 900 °C. The grain became round and large as sintering temperature increased. The grain became finally close to spherical with a smooth surface at 1000 °C. It is believed that a mass transport mechanism that began with the atomic diffusion at relatively low temperatures continued due to the additional grain boundary diffusion at high temperature.

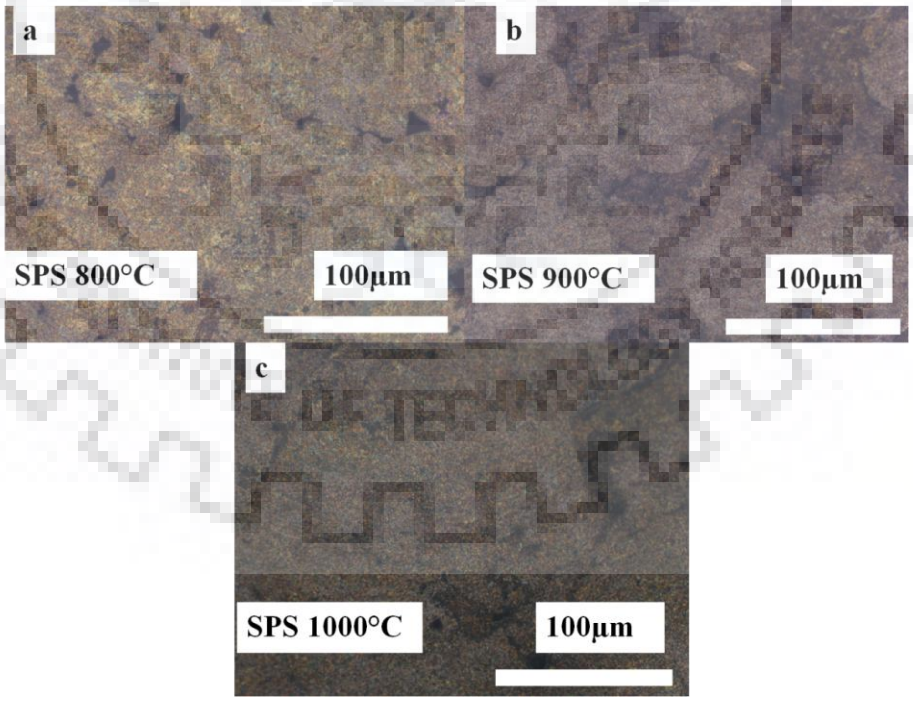

Fig. 4.6. Optical microstructures of Fe-Ni alloy sintered at (a) 800^{o}C, (b) 900^{o}C and (c) 1000^{o}C.

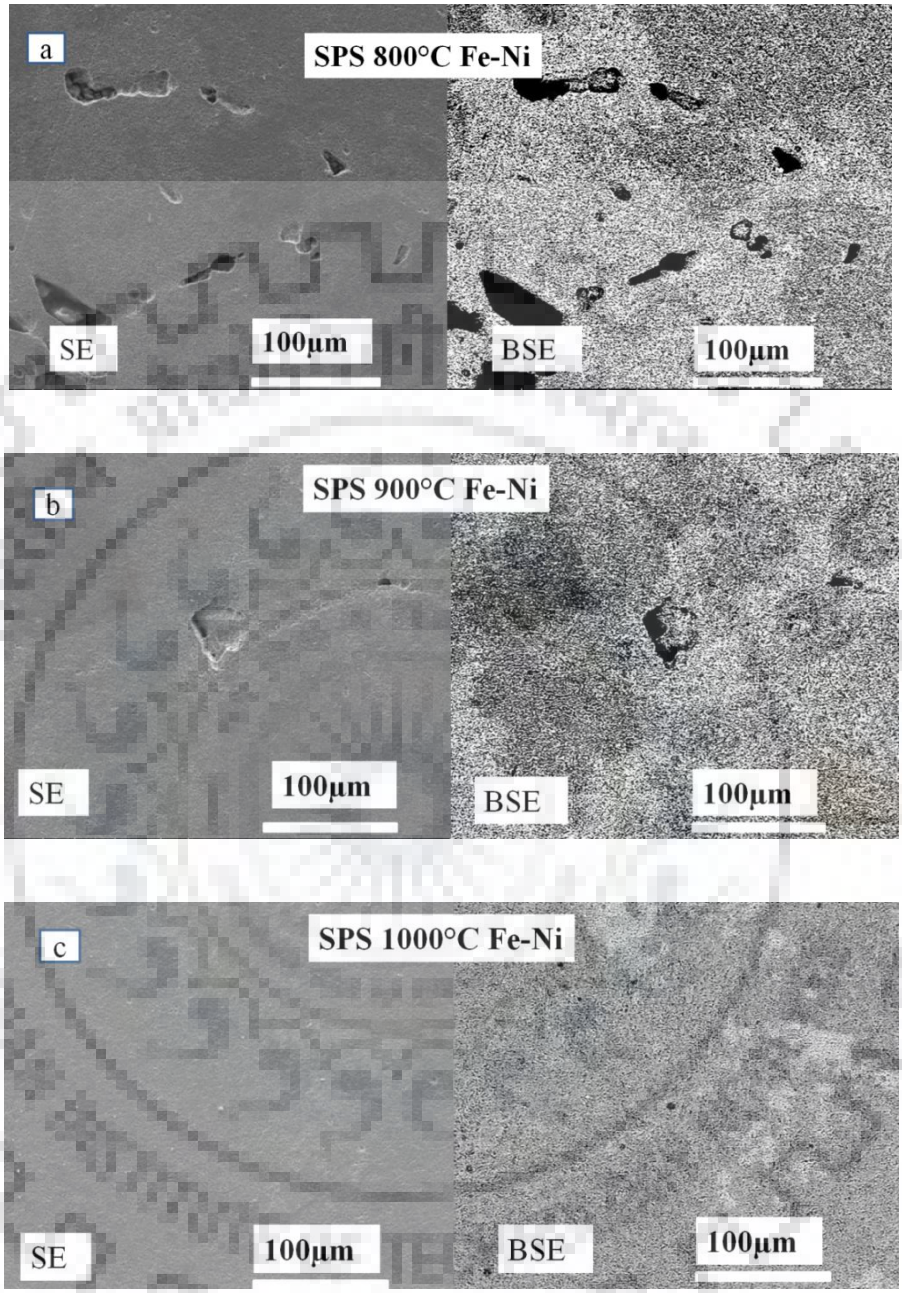

Fig. 4.7. Typical SEM images of Fe-Ni alloy sintered at (a) 800^{o}C, (b) 900^{o}C and (c) 1000^{o}C.

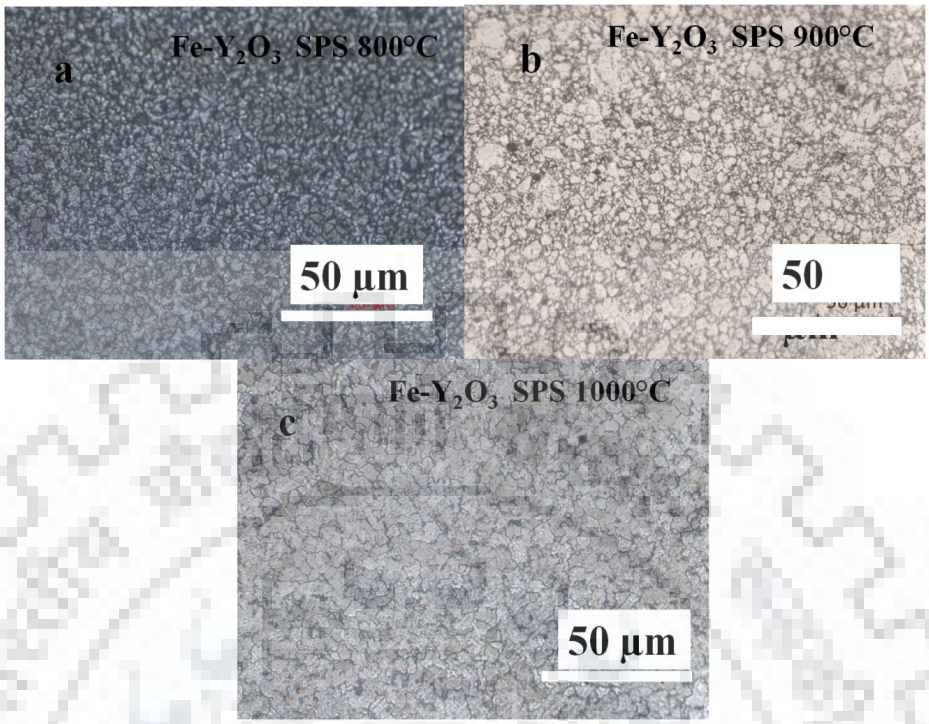

Fig. 4.8. Optical microstructures of Fe-Y_2O_3 alloy sintered at (a) 800^{o}C, (b) 900^{o}C and (c) 1000^{o}C.

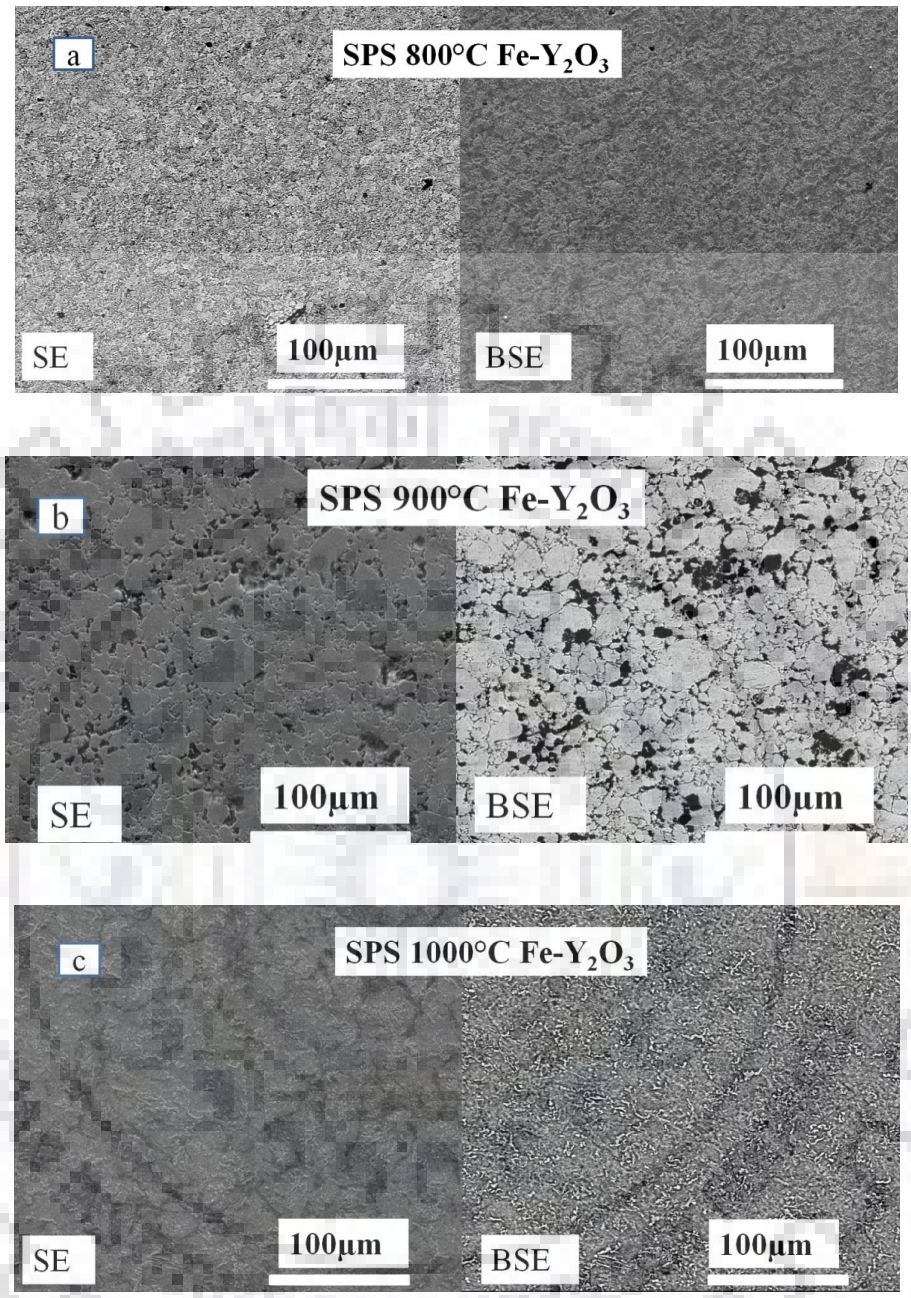

Fig. 4.9. Typical SEM images of Fe-Y_2O_3 alloy sintered at (a) 800^{o}C, (b) 900^{o}C and (c) 1000^{o}C.

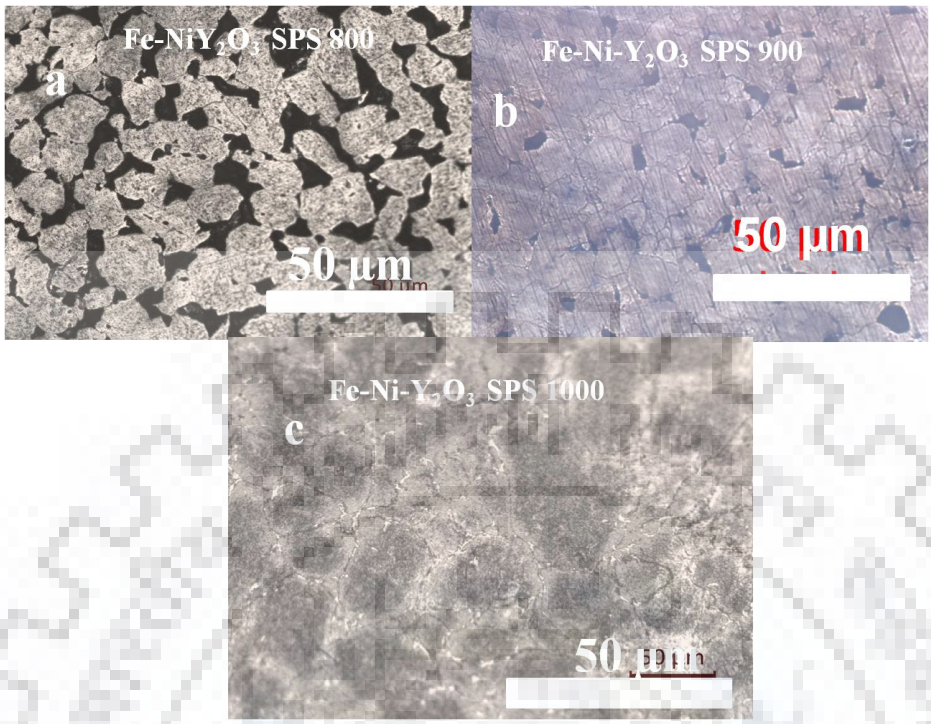

Fig. 4.10. Optical microstructures of Fe-Ni-Y_2O_3 alloy sintered at (a) 800^{o}C, (b) 900^{o}C and (c) 1000^{o}C**.**

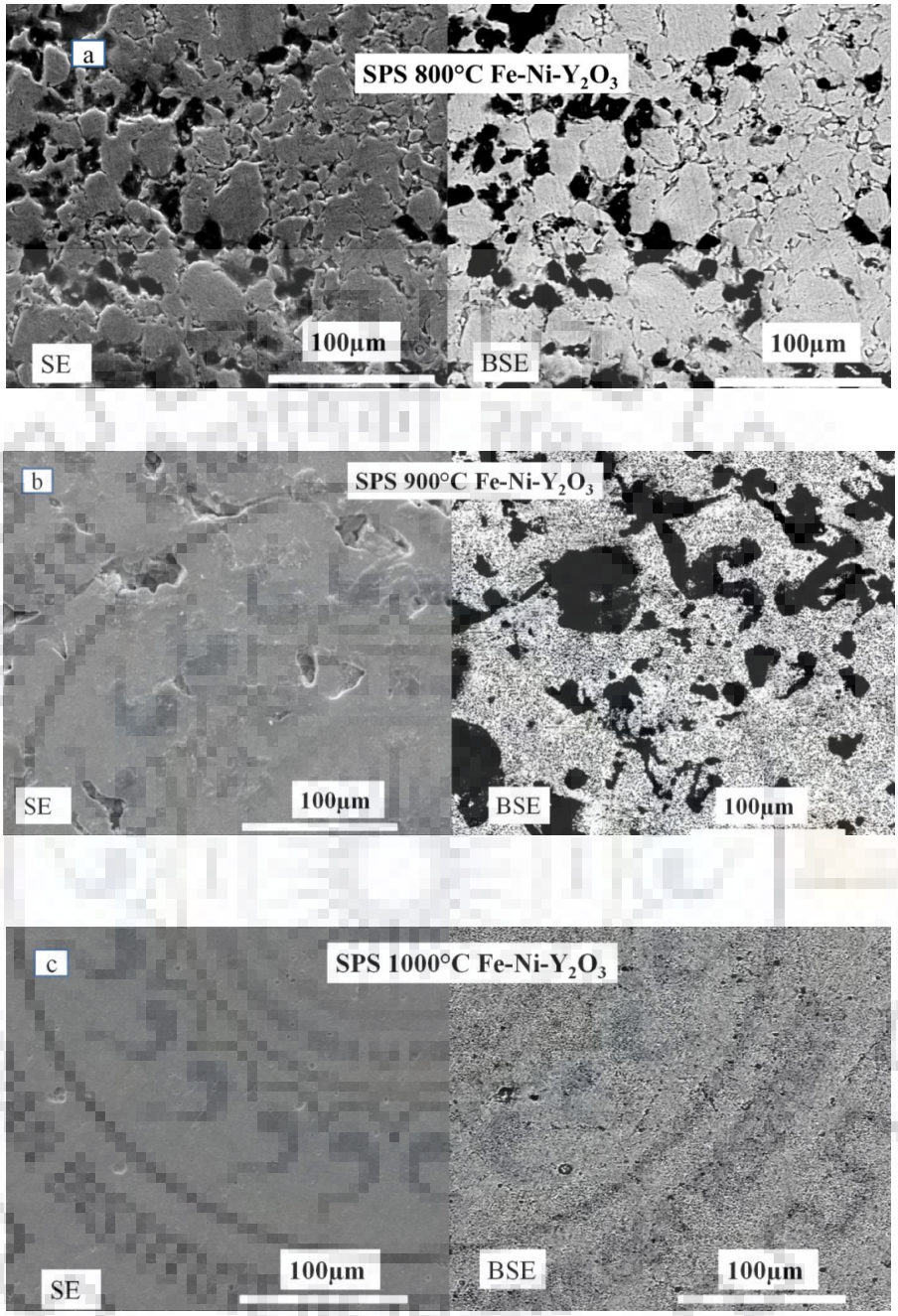

Fig. 4.11. Typical SEM images of Fe-Ni-Y_2O_3 alloy sintered at (a) 800^{o}C, (b) 900^{o}C and (c) 1000^{o}C.

Among the microstructures of investigated alloys, the Fe-Ni microstructure shows less porosity and large grain size at low sintering temperature of 800C. However, all three alloys show similar porosities when sintered at high temperature 1000^{o}C. Further increase

in sintering temperature increased grain size. Comparatively, alloys with Y_2O_3, i.e. Fe-Y_2O_3 and Fe-Ni-Y_2O_3 show refinement in grain size.

4.5 Hardness of sintered alloys

Hardness values measured by Vickers indentation are shown in **Fig. 4,12.** Vickers hardness varied from 2.5 GPa to 6.2 GPa. It is found that hardness of alloys sintered at low sintering temperatures (800°C) was high as the grain size was smaller. While comparing hardness of investigated alloys, the hardness of Fe-Ni-Y_2O_3 was more as Y_2O_3 played the role of grain refinement. Hardness of Fe-Ni is found least due to the absence of grain refinement. Though Ni also played grain refinement role, it is restricted to small extent 6- 10%. The increase in the hardness with decrease grain size can be explained through the Hall-Petch relation.

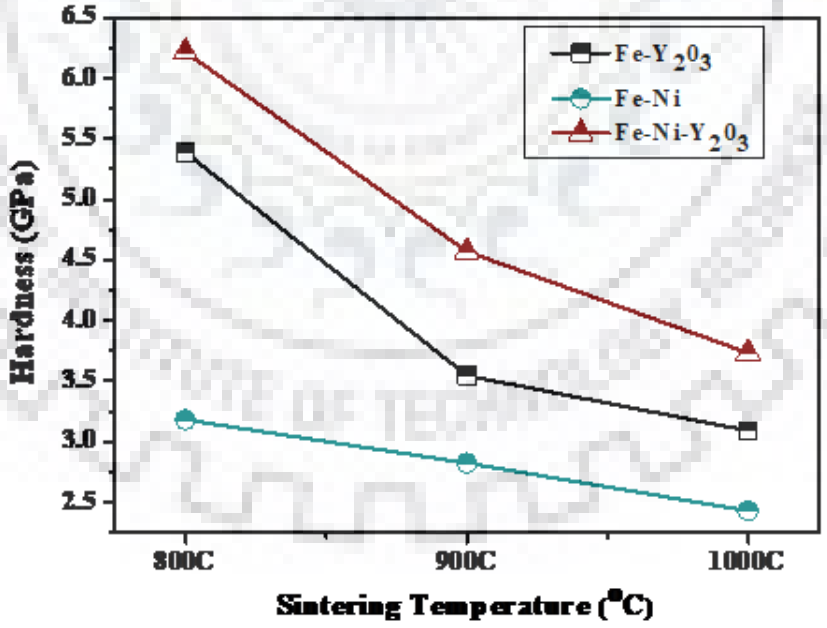

Fig. 4.12.Effect of sintering temperature and composition on Vickers hardness

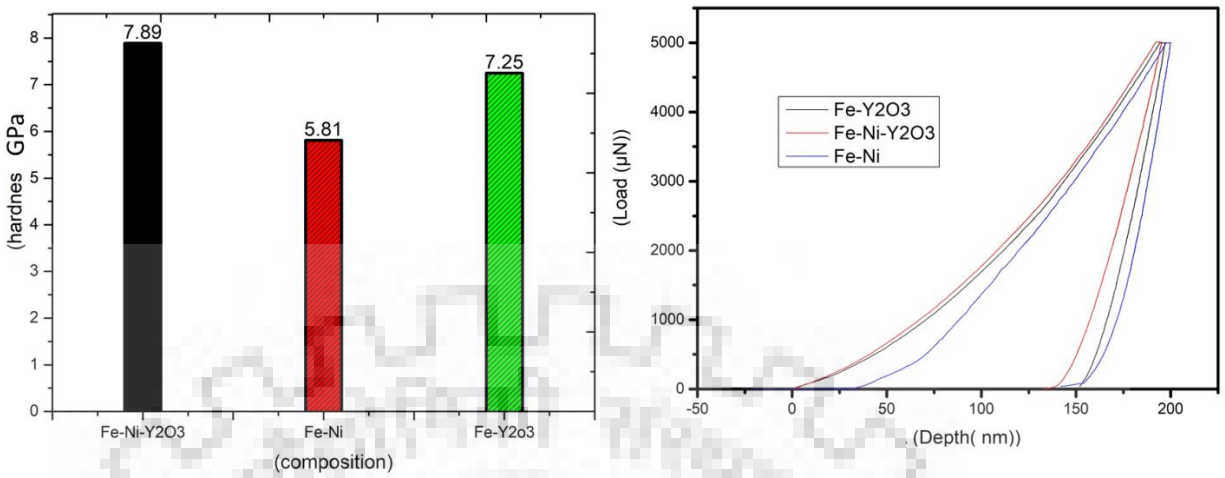

Fig 4.13. Nano indentation analysis of alloys sintered at 1000^{o}C.

The nano hardness for the investigated alloys sintered at 1000oC is shown in **Fig. 4.13.** Absolute hardness obtained from Vickers and nano indentation test are found different. But the direct comparison is not justified owing to the difference in tip geometry, measurement length scale and the vast difference in applied load. Nano indentation hardness is found to be more compare to Vickers hardness. But the trend with respect to composition of alloy sintered at 1000oC is found to be same. The Fe-Ni alloy showed minimum nano hardness of 5.81 GPa, while the Fe-Ni-Y_2O_3 alloy showed maximum nano hardness of 7.25 GPa. The depth of penetration was also minimum for Fe-Ni-Y_2O_3 alloy and maximum for Fe-Ni alloy.

4.6 Wear behavior

Ball- on- disk wear tests were performed against alumina at different loads: 5N, 10N and 20N for Fe-Ni, Fe-Ni-Y_2O_3 and Fe-Y_2O_3 alloys sintered at 1000^{o}C. The average friction coefficient (COF) varied in wide range from 0.5 to 1.7 (**Fig. 4.14**). In general, the COF decreased with increase in load. The addition of yttria in Fe or Fe-Ni decreased COF. Fe-

Ni alloy exhibited maximum COF of 1.6 at 5 N, while the Fe-Ni-Y_2O_3 alloy showed minimum COF of 0.5 at 20 N. Further, fluctuations in friction are observed for the alloys containing hard yttria in composition.

Typical surface profiles of tracks obtained after wear of alloys sintered at 1000^{o}C are shown (**Fig. 4.15**). The depth of wear track varied from 5 µm to 20 µm with change in composition of the alloy and sliding load. Fe–Ni exhibited maximum depth, while the Fe-Ni- Y_2O_3 alloy exhibited minimum depth. The wear track depth of the alloy with maximum hardness exhibited minimum wear.

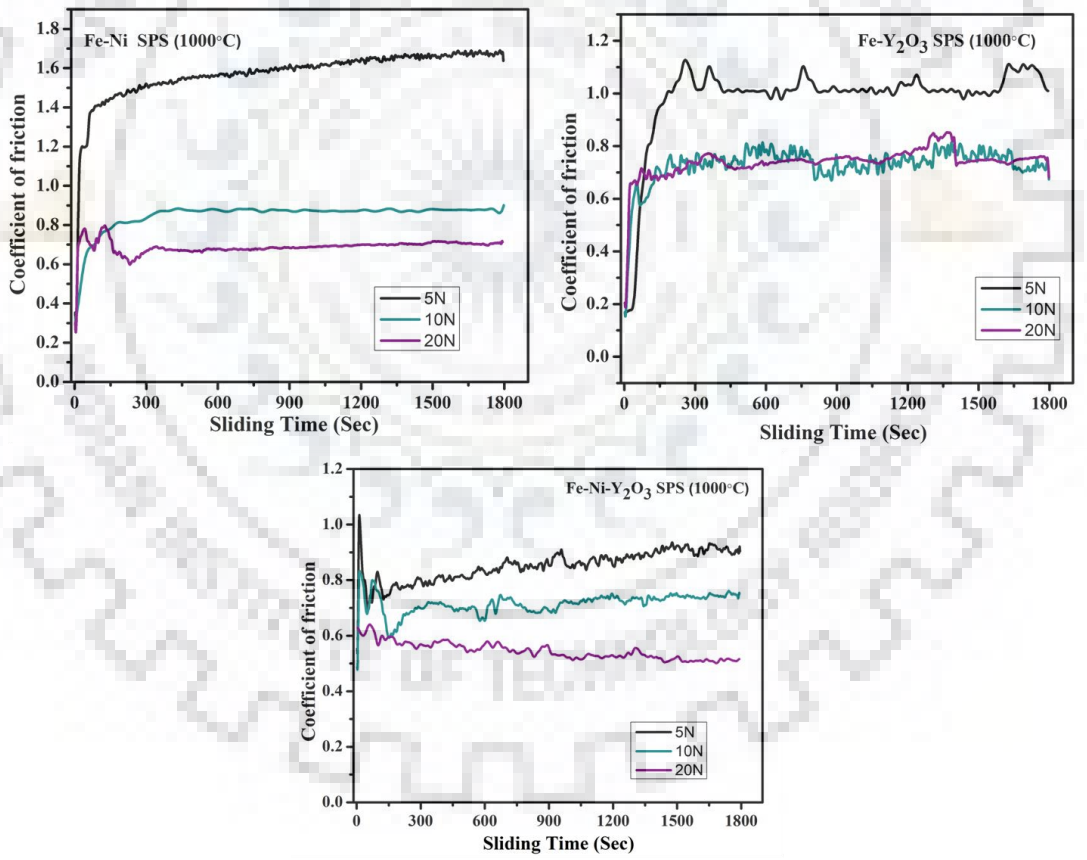

Fig. 4.14 Variation of coefficient of friction with change in load (5N to 20N) for alloys sintered at 1000°C

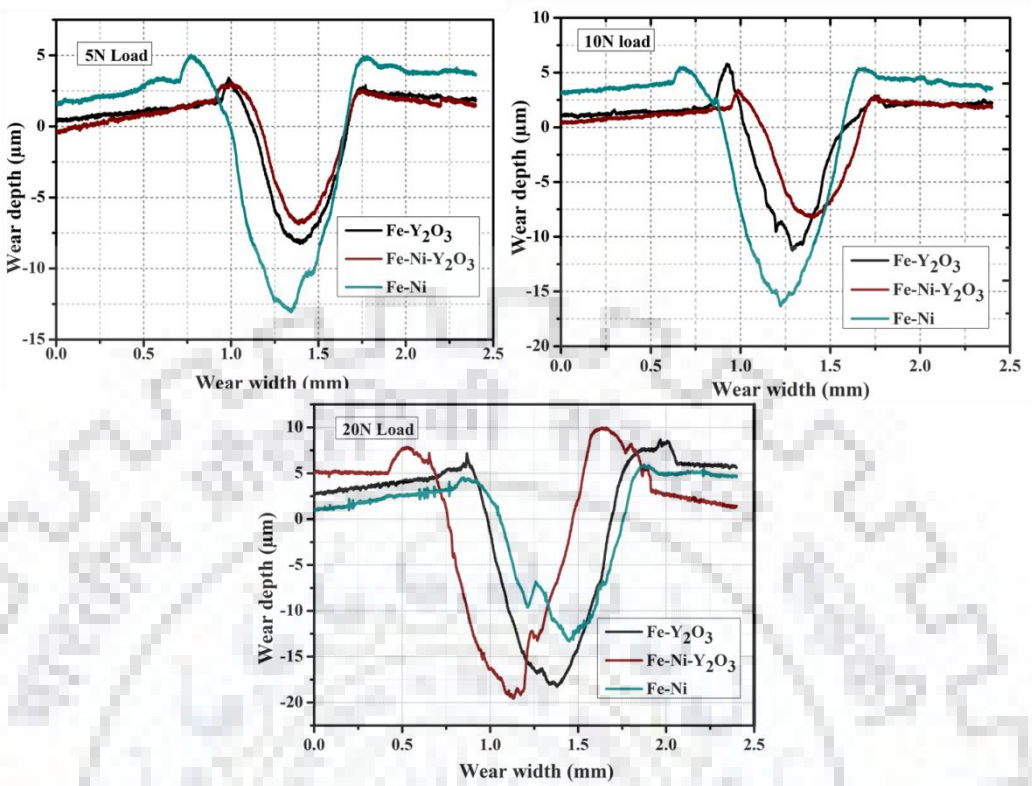

Fig. 4.15 Typical surface profiles of wear track of the alloys sintered at 1000°C.

Worn surfaces of alloys sintered at1000°C are shown in **Fig. 4.16.** In general, the worn surface of alloys showed abrasion grooves at low load of 5 N, while decreased grooves and layers observed at high load of 20 N. Fe-Ni-Y_2O_3 alloys showed relatively shallower loads at low load, while the layer completely covered the surface at high load. Thus, the dominant wear mechanisms changed from abrasion to adhesion and removal of layers with change in composition and load. As the sliding was done in ambient condition, the layers formed at high load are believed to be rich in oxides. Referring to XRD analysis (see **Fig. 4.5**) of sintered alloys, it can be said that the presence of Fe_3O_4 and NiO in case of Fe-Ni-Y_2O_3 is believed to contribute to the large extent of formation of oxide rich layer at the contact. The COF and wear depth are also minimum in case of Fe-Ni-Y_2O_3 alloy.

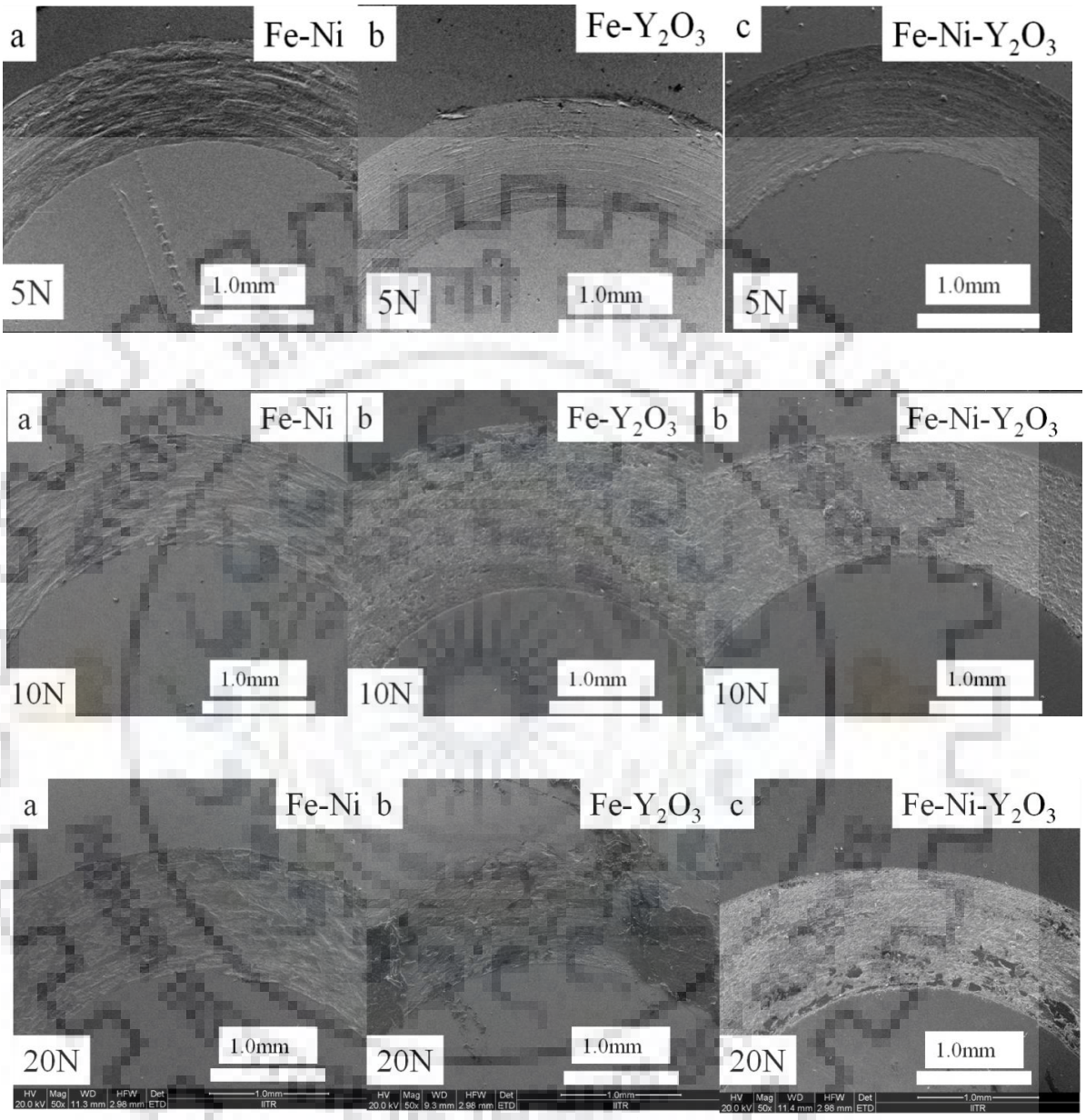

Fig. 4.16. Worn surfaces of alloys sintered at 1000°C as function of load and composition.

4.7 Corrosion behavior

Potentiodynamic polarization behavior for Fe-Ni-Y_2O_3 and Fe-Ni samples sintered 1000°C is shown as E vs.I plots in **Fig. 4.17** and details are presented in **Table 4.1**. It is found that corrosion resistance of Fe-Ni- Y_2O_3 was slightly more than Fe-Ni. The ccorrosion density (I_{corr}) decreased from 1.34 µA/cm^2 for Fe-Ni and 0.78 µA/cm^2 Fe-Ni-Y_2O_3. Appropriate addition of Y_2O_3 could decrease oxidation rate and increase adhesion between oxide scale and substrate, which is beneficial to improve exfoliation resistance of oxide scale. [25] Presence of stable oxide layer in Fe-Ni- Y_2O_3 alloy is attributed to the resistance against corrosion.

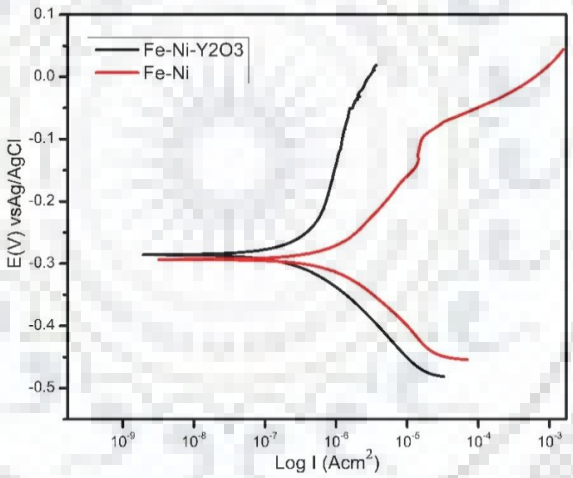

Fig. 4.17. E vs. I plots for Fe-Ni-Y_2O_3 and Fe-Ni alloys sintered at 1000°C.

Table 4.1. Results obtained from corrosion test for the alloys sintered at 1000°C.

Samples	Ecorr mV vs SCE	Icorr µA/cm^2	B_{a} V/dec	B_{c} V/dec
Fe-Ni	-293.0mV	1.34±0.40	0.158±0.03	0.121±0.03
Fe-Ni-Y_2O_3	-288.0mV	0.78±0.04	1.054±0.04	0.155±0.02

CHAPTER 5 CONCLUSIONS AND FUTURE SCOPE

Major conclusions obtained from the present experimental investigation of preparation and characterization of yttria added Fe-Ni alloys are provided. This is followed by directions for future studies.

As received yttria powder was milled for 40h to reduced the particle size to 20 -30 nm. The mixed powders of Y2O3, Ni and Fe were sintered by spark plasma sintering at 800^{o}C, 900^{o}C and 1000^{o}C. The density of sintered samples increased with increase in sintering temperature. The addition of Y_2O_3 caused decrease in crystalline size. As the sintering temperature is increased the hardness of alloys decreased. Addition of Y_2O_3 increased hardness about 35% from 5.8 GPa up to 7.9 GPa. Fe–Ni exhibited maximum wear in sliding against alumina ball, while the Fe-Ni- Y_2O_3 alloy exhibited minimum wear. Corrosion resistance of Fe-Ni-Y_2O_3 was slightly more than Fe-Ni. The present research essentially indicates the effect of addition of ytrria on mechanical, wear and corrosion behaviour of iron-nickel alloy.

The addition of yttria can be varied and the sinterability and microstructural characterization can be studied in future. The mechanical properties like hardness, strength and ductility can be studied as function of yttria. The performance of yttia added iron-nickel alloy in wear and corrosion condition can be studied as function of alloy composition and test parameters.

CHAPTER 6 REFERENCES

[1] D. mutter, C. Schieback, J. Nedar, F. Burzale, K. Franzrahe, A. Gerg and P. Nielaba, Numeriacal studies of structures and phases in nano system in reduced geometry. NIC Symposium 2010: Proceedings, 24 - 25 February 2010, Jülich, Germany.

[2] M. Aronniemi, J. Sainio, J. Lahtinen, Chemical state quantification of iron and chromium oxides using XPS, the effect of the background subtraction method. Surface Science, 579 (2005) 108-123.

[3] K.A Darling, B.K. VanLeeuwen, J.E. Semones, C.C. Koch, R.O. Scattergood, L.J. Kecskes, S.N. Mathaudhu, Stabilized nanocrystalline iron-based alloys. Materials Science and Engineering A 528 (2011) 4365– 4371

[4] LIU Dong-hua, LIU Yong, ZHAO Da-peng, WANG Yan, FANG Jing-hua, WEN Yuren, LIU Zu-ming, Effect of ball milling time on microstructures and mechanical properties of mechanically-alloyed iron-based materials. Transactions Nonferrous Met. Soc. China 20(2010) 831-838

[5] H. Kotan, M. Saber, C.C. Koch, R.O. Scattergood, Effect of annealing on microstructure, grain growth, and hardness of nanocrystalline Fe–Ni alloys prepared by mechanical alloying H. Kotan, M. Saber, C.C. Koch, R.O. Scattergood, Materials Science and Engineering A 552 (2012) 310– 315

[6] D. Cui, J. Jiang, G. Cao, E. Xiao, X. Qu, J, Stabilisation of Fe based nano-structures developed through mechanical milling. Univ. Sci. Technol. Beijing 15 (2008) 150–154.

[7] C. C. Koch , Synthesis of nanostructured materials by mechanical milling: problems and opportunities, nanostructured materials. vol. 9. pp. 13-22.1997

[8] M.A. Meyers, A. Mishra, D.J. Benson, Prog, Mechanical properties of nanocrystalline materials. Mater. Sci. 51 (2006) 427–556.

[9] C. Suryanarayana. Mechanical alloying and Milling, Progress in Materials Science. 46 (2001): pp. 1-184

[10] D Nayak, S Mula, Analysis and optimization of Material removal rate and Surface Roughness of AISI D2 after EDM process, Processing and fabrication of advanced materials XXI, IIT Guwagati, December 2012, page 931-937

[11] Olive A. Graeve Spark plasma sintering of Fe- based SAM with Y_2O_3 nanoparticle addition, Material letters 62 (2008) 2988-2991.

[12] E.K. Park, An investigation on stability of Y_2O3 and sintering behavior of Fe-base ODS particles prepared by high energy ball milling. 2012 18^{th} international Conference on composite materials

[13] J.L. McCrea Red, Properties and applications for electrodeposited Nano crystalline Fe-Ni alloys. Adv.Mater.Sci. 5 (2003) 252-258

[14] Hasan Kotan, Study of grain growth in a Nano crystalline Fe91Ni8Zr1 alloy. Journal of material science (2013) 48:2251-2257

[15] Hasan Kotan, Effect of zirconium on grain growth and mechanical properties of ball- milled Nano crystalline Fe-Ni alloy. Journal of alloys and compounds 551 (2013) 621-629

[16] Hasan Kotan, Influence of Zr and nano-Y_2O_3 additions on thermal stability and improved hardness in mechanically alloyed Fe based ferritic alloys. Journal of alloys and compounds 615 (2014) 1013-1018.

[17] Mxolisi Brendon Shongwe, Effect of sintering temperature on the microstructure and mechanical properties of Fe-30%Ni alloys produced by spark plasma sintering, J. alloys and compounds 649 2015 (824-832).

[18] HEBM B.S. Murthy, Microstructural studies on nanocrystalline oxide dispersion strengthened austenitic (Fe-18Cr-8Ni-2W-0.25Y_2O_3) alloy synthesized, Journal of Material science (2010) 45:4858-4865.

[19] LIU Ye. J. Cent, Solution combustion synthesis of Fe−Ni−Y_2O_3 nanocomposites for magnetic application, South Univ. (2015) 22: 23−29.

[20] Isaac Moraka Mokena, Influence of Temperature on Microstructure and Mechanical properties of Ni-40Fe-10Co Alloy Consolidated by Spark Plasma Sintering. International conference of sustainable materials and processing manufacturing 23-25 January 2017.

[21] Nuraine Mariana Md. Shahrani, Effect of sintering temperature on crystallography and microstructure of yttrium iron garnet via mechanical alloying technique , Journal of Solid St. Sci. & Technol. Letters, 2015, Vol. 16 No. 1-2, pp. 67-72.

[22] Yu. I. Ustinovshchikov, Microstructures Responsible for the Invar and Permalloy Effects in Fe–Ni Alloys, published in Metally, 2015, No. 3, pp. 60–66.

[23] M. Brendon Shongwe, Effect of Sintering Temperature on the Microstructure and Mechanical Properties of Fe-30%Ni Alloys Produced by Spark Plasma Sintering, DOI: 10.1016/j.jallcom.2015.07.223.

[24] R.J Young, Densification and microstructure development in the reaction sintering process of yttrium iron garnet, journal of materials science 25 (1990) 3566-3572.

[25] D. Sun, Effect of Y_2O_3 contents on oxidation resistance at 1150◦C and mechanical properties at room temperature of ODS Ni-20Cr-5Al alloy, Applied Surface Science 385 (2016) 587–596.

[26] Neera Singh, Om Parkash, Devendra Kumar, Phase evolution, mechanical and corrosion behavior of Fe(100-x) Ni(x) alloys synthesized by powder metallurgy,

[27] Olivia A. Graeve, Spark plasma sintering of Fe-based structural amorphous metals with Y_2O_3 nanoparticles additions., Materials letters 62 (2008) 2988-2991